

Observation of Topological Hall Effect and Signature of Room Temperature Antiskyrmions in Mn-Ni-Ga D_{2d} Heusler magnets

Subir Sen,^{1,*} Charanpreet Singh,^{1,*} Prashanta K. Mukharjee,² Ramesh Nath,² and Ajaya K. Nayak^{1,†}

¹*School of Physical Sciences, National Institute of Science Education and Research, HBNI, Jatni-752050, India*

²*School of Physics, Indian Institute of Science Education and Research, Thiruvananthapuram, Kerala-695551, India*

(Dated: April 4, 2019)

Topologically stable nontrivial spin structures, such as skyrmions and antiskyrmions, display a large topological Hall effect owing to their quantized topological charge. Here, we present the finding of a large topological Hall effect beyond room temperature in the tetragonal phase of a Mn-Ni-Ga based ferrimagnetic Heusler shape memory alloy system. The origin of the field induced topological phase, which is also evidenced by the appearance of dips in the ac-susceptibility measurements, is attributed to the presence of magnetic antiskyrmions driven by D_{2d} symmetry of the inverse Heusler tetragonal phase. Detailed micromagnetic simulations asserts that the antiskyrmionic phase is stabilized as a result of interplay among inhomogeneous Dzyaloshinskii-Moriya interaction, the Heisenberg exchange, and the magnetic anisotropy energy. The robustness of the present result is demonstrated by stabilizing the antiskyrmion hosting tetragonal phase up to a temperature as high as 550 K by marginally varying the chemical composition, thereby driving us a step closer to the realization of ferrimagnetic antiskyrmion based racetrack memory.

PACS numbers: 75.50.Gg, 75.50.Cc, 75.30.Gw, 75.70.Kw

Keywords: Topological Hall Effect, Skyrmions, Heusler compounds

In recent years, there is a significant interest towards non-collinear magnetism, where the local magnetic state can be *periodically* altered via spin transfer torque by passing a spin polarized current [1]. The prospect of non-collinear magnetism can be greatly enhanced when the aforementioned magnetic structure is topologically stable in nature. One of such spin textures is the recently discovered magnetic skyrmion, which is a vortex-like object with a swirling spin configuration [2, 3]. The topological nature of the skyrmions helps them to get decoupled from the crystal lattice, thereby assisting to move at much lower current density in comparison to that of domain walls [4]. The topologically stable spin texture of the skyrmions is accompanied by a topological charge $Q = \frac{1}{4\pi} \int \mathbf{m} \cdot (\frac{\partial \mathbf{m}}{\partial x} \times \frac{\partial \mathbf{m}}{\partial y}) dx dy = \pm 1$, where \mathbf{m} is the unit vector along the local magnetization [5]. When a conduction electron approaches a skyrmion, the spin of the electron tries to align with the local magnetization of the skyrmion owing to a large Hund's coupling. Consequently, the electrons experience a large fictitious magnetic field, resulting in an additional component to the observed Hall voltage, named as topological Hall effect (THE) [12]. Effective fictitious magnetic field of 4000 T can be realized for a skyrmion of size 1 nm [8]. Depending upon the topological charge of the skyrmion (± 1), the topological Hall component adds or subtracts from the normal and anomalous Hall components to develop a hump or dip type of behavior in the total Hall voltage observed in various bulk materials and thin films [4, 6–12].

The topologically stable spin texture of the skyrmions arises from the spin-orbit interaction mediated Dzyaloshinskii-Moriya interaction (DMI), which com-

petes with the Heisenberg exchange (J) and magnetic anisotropy to form a stable skyrmion lattice. The DMI energy that can be expressed as $\mathbf{D}_{ij} \cdot (\mathbf{S}_i \times \mathbf{S}_j)$, where D is the DMI vector and S_i and S_j are spins at the i^{th} and j^{th} sites, respectively, exists in systems with broken inversion symmetry and large spin-orbit coupling [13, 14]. The magnetic materials with B20 and related crystal classes that possess intrinsic bulk DMI display Bloch-type skyrmions [2, 3, 15–17], whereas, most of the layered thin films with interfacial DMI and some bulk materials with suitable crystal symmetry host Néel skyrmions [18–24]. Artificial magnetic skyrmions with nano-patterning is also realized without DMI [25–27]. A latest addition to the skyrmion family is the recently observed antiskyrmions in D_{2d} crystal symmetry based inverse tetragonal Heusler compounds [28]. The special crystal symmetry of these materials ensures an inhomogeneous DMI vector ($D_x = -D_y$) in contrast to the homogeneous DMI observed in materials exhibiting Bloch and Néel skyrmions ($D_x = D_y$) [29–31].

It has been established that Mn_2YZ -based Heusler compounds display a non-centrosymmetric crystal structure [32]. The DMI in these materials can be set up in case of Mn_2YZ tetragonal Heusler compounds [28, 33]. The Heusler shape memory alloys (SMA) that undergo a martensite transition from high temperature cubic to low temperature tetragonal phase, possess a great potential to host nontrivial spin texture like skyrmions. However, most of these alloys exhibit a modulated and centrosymmetric tetragonal structure that preclude DMI in the system [34–36]. An asymmetric tetragonal structure with D_{2d} symmetry can be stabilized in case of Mn_2NiGa when a single Mn atom in the Mn-Mn plane is replaced by Ni atom in Mn_3Ga , as shown in Fig. 1(a) [37–40].

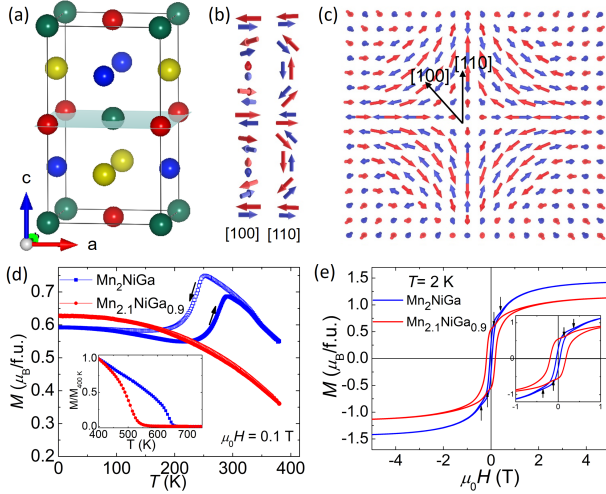


FIG. 1. (Color online) (a) Crystal structure of Mn_2NiGa : MnI, Ga, MnII and Ni atoms are represented by red, green, blue and yellow balls, respectively. The ab -plane is shown in light green color. (b) Schematic representation of one-dimensional spin propagation along $[100]$ (helix) and $[110]$ (cycloid) in the ab -plane. (c) Spin configuration of a ferrimagnetic antiskyrmion in the present system. (d) Field cooled (FC) and field heating (FH) temperature dependence of magnetization $[M(T)]$ for Mn_2NiGa and $\text{Mn}_{2.1}\text{NiGa}_{0.9}$ measured in 0.1 T field. Inset shows the high temperature $M(T)$ curves showing the Curie temperature (T_C). (e) Field dependent magnetization $[M(H)]$ loops measured at 2 K for Mn_2NiGa and $\text{Mn}_{2.1}\text{NiGa}_{0.9}$. The inset shows low field region of the data.

The Mn sitting in Mn-Mn/Mn-Ni plane and the Mn at Mn-Ga plane align antiferromagnetically, account for the ferrimagnetic ordering in the system [41]. The existence of a more complex non-collinear spin structure and/or the presence of slight antisite disorder intrinsic to most of the Heusler materials can also result in the mismatch between experimentally observed moment with that of theoretical prediction [41]. In this letter we show that Mn-rich Mn-Ni-Ga based inverse Heusler system indeed displays a large topological Hall effect in the tetragonal phase, suggesting the presence of antiskyrmions in the system.

Like most of the Mn_2 -based Heusler compounds, Mn_2NiGa exhibits a ferrimagnetic ordering with a Curie temperature of ~ 650 K. The D_{2d} symmetry of the tetragonal phase can ensure a competing interaction between the DMI and the Heisenberg exchange that can result in an one-dimensional helix in the $[100]$ direction and a cycloid along the $[110]$ direction, as shown in Fig. 1(b). In this scenario, application of magnetic field can generate ferrimagnetic antiskyrmions as schematically demonstrated in Fig. 1(c). The thermomagnetic $M(T)$ curves measured in field-cooled (FC) and field-heating (FH) modes up to 400 K for Mn_2NiGa and $\text{Mn}_{2.1}\text{NiGa}_{0.9}$ are depicted in Fig. 1 (d). The signature of structural

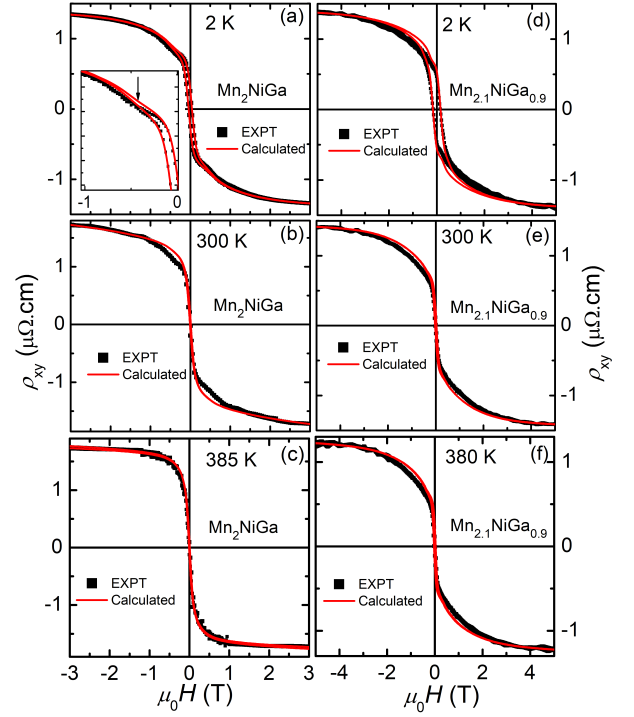


FIG. 2. (Color online) Field dependent Hall resistivity (ρ_{xy} , filled squares) measured at different temperatures for (a)-(c) Mn_2NiGa , (d)-(f) $\text{Mn}_{2.1}\text{NiGa}_{0.9}$. The inset of (a) shows an expanded view of the ρ_{xy} in the second quadrant. The solid lines represent calculated Hall resistivity without topological Hall contribution as described in the text.

transition in Mn_2NiGa can be seen from the presence of large hysteresis in cooling and heating $M(T)$ curves around 300 K, whereas, no such transition is found in $\text{Mn}_{2.1}\text{NiGa}_{0.9}$. Both the samples exhibit the Curie temperature (T_C) well above the room temperature [inset of Fig. 1(d)]. An experimental signature that hints at the presence of an additional magnetic phase in both the samples was obtained from the isothermal magnetization $M(H)$ data which display a small kink marked by arrows in Fig. 1(e). Since Mn_2NiGa transforms to the cubic phase above 300 K, this transition disappears for $M(H)$ loops measured at higher temperatures. The magnetic moment of the present Mn_2NiGa matches well with the previous report [38].

Motivated by the signature of magnetic phase transition in the $M(H)$ data, we have performed Hall effect measurements at different temperatures as depicted in Fig. 2. For Mn_2NiGa , the total Hall resistivity ρ_{xy} exhibits a dip around 0.5 T for all temperatures $T \leq 300$ K [Fig. 2(a)&(b)]. This peculiar behavior disappears for the ρ_{xy} data collected above the martensite transition at $T = 385$ K in the cubic phase [Fig. 2(c)]. Although the martensite transition sets the DMI in the tetragonal phase, it has no role in the observed anomaly in the ρ_{xy} data. This is demonstrated in another sample

$\text{Mn}_{2.1}\text{NiGa}_{0.9}$ that exhibits tetragonal phase in the whole temperature range up to the T_C , without any structural transition. For this sample the ρ_{xy} data acquired up to 380 K, the highest possible measured temperature, display a similar dip kind of behavior around 1 T [Fig. 2(d)-(f)].

It is well known that the total Hall resistivity can be expressed as $\rho_{xy} = \rho_N + \rho_{AH} + \rho_{xy}^T$, where ρ_N , ρ_{AH} and ρ_{xy}^T are normal, anomalous, and topological Hall resistivities, respectively. Normal Hall resistivity can be written as $\rho_N = R_0 H$, where R_0 is the normal Hall coefficient. Anomalous Hall resistivity, which is in general directly proportional to the magnetization in a ferri-/ferromagnet, can be expressed in terms of the longitudinal resistivity (ρ_{xx}) and magnetization (M) as $\rho_{AH} = b\rho_{xx}^2 M$, where b is a constant. The effect of skew scattering and side-jump on AHE in the present sample are not taken into consideration due to the fact that the longitudinal resistivity in the present bulk materials is too high and can be neglected completely at high temperatures. In case of Mn_2NiGa , the anomaly in the ρ_{xy} data is only found for fields less than 1 T, whereas, $\text{Mn}_{2.1}\text{NiGa}_{0.9}$ displays such behavior for fields up to 2 T. Hence it is assumed that the high field ρ_{xy} data do not consist of any ρ_{xy}^T component. At high fields, ρ_{xy} can be further simplified to $\rho_{xy} = R_0 H + b\rho_{xx}^2 M$. The linear fit between $\frac{\rho_{xy}}{H}$ and $\frac{\rho_{xx}^2 M}{H}$ gives us slope b and intercept R_0 . In the present case, the values of b and R_0 are calculated by using ρ_{xy} data for $\mu_0 H > \pm 3$ T. Afterwards, ρ_{xy} sans ρ_{xy}^T was calculated using $\rho_{xy} = R_0 H + b\rho_{xx}^2 M$, as shown by red lines on the top of the experimental ρ_{xy} curves in Fig. 2. It can be clearly seen that the experimental and the calculated ρ_{xy} curves display a substantial difference at the field where both the magnetization and Hall resistivity exhibit dips, whereas, perfect matching is obtained for higher field regions. The calculated ρ_{xy} was subtracted from the experimental ρ_{xy} to obtain ρ_{xy}^T as plotted in Fig. 4(a)&(b). The validity of the extraction of THE by the present method is well verified in case of $\text{Mn}_{1.8}\text{Ni}_{1.2}\text{Ga}$, where both the experimental and calculated curves match at all field regime, as this sample does not exhibit any anomaly in Hall effect measurements.

For a deep understanding of the origin of the observed topological Hall effect, we have carried out ac-susceptibility measurements which have been extensively used to characterize skyrmions in several materials [24, 44, 45]. In the present case, the real part of the ac-susceptibility, $\chi'(H)$, for Mn_2NiGa exhibits a dip/peak type behavior around the fields where a large topological Hall effect is found. The magnitude of this dip/peak behavior initially increases with increasing temperature before getting slowly suppressed for $T \geq 250$ K due to the presence of a small amount of cubic phase with higher magnetic susceptibility. The dip/peak completely vanishes at 370 K in the cubic phase. For $\text{Mn}_{2.1}\text{NiGa}_{0.9}$, a

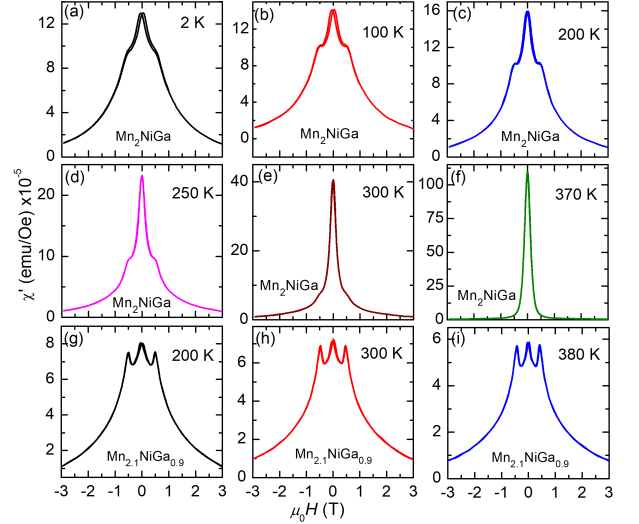


FIG. 3. (Color online) Field dependent ac-susceptibility measured at different temperatures for; (a)-(f) Mn_2NiGa and (g)-(i) $\text{Mn}_{2.1}\text{NiGa}_{0.9}$.

pronounced and well defined dip/peak can be found up to 380 K, suggesting the presence of magnetic antiskyrmions in the present system. It is worth to mention that the tetragonal Heusler compound $\text{Mn}_{1.4}\text{Pt}_{0.9}\text{Pd}_{0.1}\text{Sn}$ that displays antiskyrmions up to room temperature [28] also exhibits a similar behavior in the ac-susceptibility data [46]. The robustness of the ac-susceptibility measurements is vindicated in case of $\text{Mn}_{1.8}\text{Ni}_{1.2}\text{Ga}$ that does not exhibit any anomaly in $\chi'(H)$ as no THE is found in this sample.

The occurrence of large topological Hall effect that is underpinned by the observation of dips/peaks in the ac-susceptibility data in the present material lends firm support for the existence of some non-trivial spin texture, such as, skyrmions. The D_{2d} crystal symmetry of the present system ensures an anisotropic DMI with $D_x = -D_y$, thereby leading to antiskyrmions. In order to gain more insights into the magnetic field and temperature dependence of the antiskyrmions in the present system, we have plotted ρ_{xy}^T at different magnetic fields as shown in Fig. 4(a)&(b). In general, the topological Hall effect scales (i) directly with the density and (ii) inversely with the size of the skyrmions/antiskyrmions. Since for a given system the size of the skyrmions/antiskyrmions remains almost constant, the enhanced ρ_{xy}^T at room temperatures for Mn_2NiGa can be attributed to a significant increase in antiskyrmion density due to the higher nucleation ability of antiskyrmions at the tetragonal to cubic phase transition. This can be understood from the fact that in case of a bulk system the nucleation probability of skyrmions/antiskyrmions increases around the magnetic ordering temperature [2, 15, 17, 28]. In case of $\text{Mn}_{2.1}\text{NiGa}_{0.9}$, the magnitude of ρ_{xy}^T almost re-

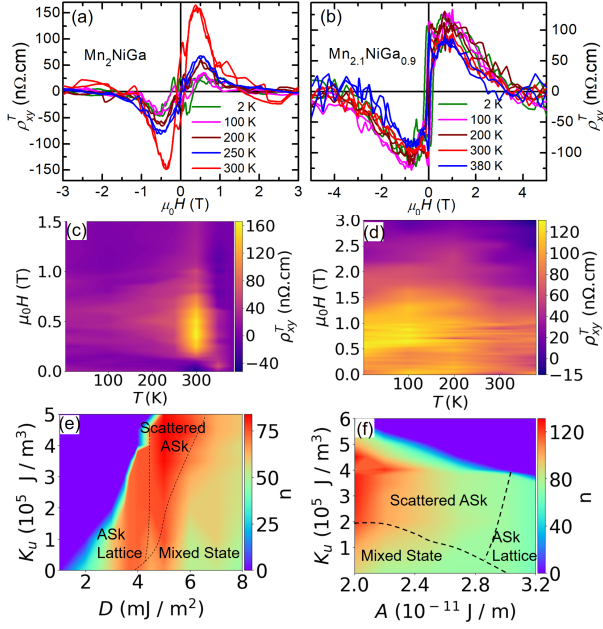


FIG. 4. (Color online) Field dependent topological Hall resistivity (ρ_{xy}^T) at different temperatures for (a) Mn_2NiGa and (b) $\text{Mn}_{2.1}\text{NiGa}_{0.9}$. The $H - T$ phase diagram showing field dependence of ρ_{xy}^T at different temperatures derived from the topological Hall effect measurements for (c) Mn_2NiGa and (d) $\text{Mn}_{2.1}\text{NiGa}_{0.9}$. (e) Magnetic anisotropy K_u versus DMI, (f) K_u versus exchange stiffness constant (A), phase diagrams illustrating the stability of antiskyrmion (ASx) phase for different K_u , D and A values. Dotted lines represent boundary between different phases. Different colors in the phase diagram represent number density of antiskyrmsions (n).

mains constant up to the highest measured temperature of 380 K. Figure 4(c)&(d) represent the $H - T$ phase diagrams for Mn_2NiGa and $\text{Mn}_{2.1}\text{NiGa}_{0.9}$. For Mn_2NiGa the THE almost vanishes for a field of about 1.5 T, whereas, $\text{Mn}_{2.1}\text{NiGa}_{0.9}$ exhibits THE for field as high as 3 T.

A factor that significantly contributes to the size and stability of the antiskyrmsions in the present tetragonal materials is the anisotropy energy. The presence of considerable amount of magnetic anisotropy in the present system can be seen from the out-of-plane type hysteretic behavior of the $M(H)$ loop in Fig. 1(d). A slight change in the Mn/Ga ratio significantly changes the coercive field and the magnetic ordering temperature. This signifies a considerable change in the magnetic anisotropy as well as the exchange constant J , which can modify the size and stability of the antiskyrmion phase. For a detailed understanding of the stability of antiskyrmion phase at different anisotropy constant K_u , DMI constant D ($D_x = -D_y$), and exchange stiffness constant A , we have carried out a detailed micromagnetic simulation using public domain software package Object Oriented Micromagnetic Framework (OOMMF) [42] with DMI ex-

tension module [43]. Initially, a $1000 \times 1000 \times 2 \text{ nm}^3$ thin film was relaxed from a random magnetization state in presence of perpendicular magnetic field for different values of D and A with zero anisotropy. A was calculated from the T_C and saturation magnetization M_s from $M(H)$ loop at 2 K. After the initial relaxation, the anisotropy constant K_u was increased to various values to check the stability of antiskyrmion lattice at the corresponding values of D , A and K_u . Figure 4(e) shows the $K_u - D$ phase diagram corresponding to the experimental parameters $A = 3.0 \times 10^{-11} \text{ J/m}$, $M_s = 2.37 \times 10^5 \text{ A/m}$, and $\mu_0 H = 500 \text{ mT}$. A stable antiskyrmion lattice can be found for $D \approx 2.0 - 4.0 \text{ mJ/m}^2$ and $K_u \approx 0 - 5 \times 10^5 \text{ J/m}^3$. A rough estimation of the anisotropy constant from the $M(H)$ loops yields $K_u \approx 3.0 - 5.0 \times 10^5 \text{ J/m}^3$. A higher D and K_u results in a mixed or scattered antiskyrmion phase. For a fixed $D = 4.0 \text{ mJ/m}^2$, a stable antiskyrmion lattice can be found for $A \approx 3.0 \times 10^{-11} \text{ J/m}$ [Fig. 4(f)]. At lower values of A , which is expected for $\text{Mn}_{2.1}\text{NiGa}_{0.9}$, mixed phase and scattered antiskyrmsions were stabilized at higher values of K_u . A decrease in the size of antiskyrmsions at lower A and higher K_u leads to a significant increase in the density (n) even in the mixed and scattered antiskyrmion state.

As it can be seen, a stable antiskyrmion phase can be formed for $D = 2.0 - 4.0 \text{ mJ/m}^2$ and $K_u = 0 - 5 \times 10^5 \text{ J/m}^3$. The size (diameter) of the antiskyrmsions corresponding to these values of D and K_u is about 40-60 nm. It is known that the magnitude of topological Hall voltage greatly depends upon the size and density of skyrmions. We have estimated the size of the antiskyrmsions from the measured topological Hall effect using the relation $\rho_{xy}^T = PR_0B_{eff}$, where P is the conduction electron spin polarization and B_{eff} is the effective (fictitious) magnetic field [12]. Further B_{eff} can be expressed as $B_{eff} = -\phi_0/a_{sk}$, with $\phi_0 = h/e$ is the magnetic flux generated by a single skyrmion and a_{sk} is the size of the skyrmion [8]. The conduction electron polarization can be roughly estimated as $P = M_{sp}/M_s$, where M_{sp} is the ordered moment in the antiskyrmion phase and M_s is the saturation magnetic moment in the system [12]. In the present case P comes about 0.7. By taking the highest THE at room temperature for Mn_2NiGa , the effective magnetic field is calculated as 8.8 T and the size of the antiskyrmsions is found to be about 22 nm. A small mismatch of the antiskyrmion size might be arising from the fact that the simulations were carried for a thin film, whereas, experiments were performed on the bulk materials. It is worth to mention here that the size of the antiskyrmsions in Mn-Ni-Ga system is much smaller in comparison to the recently observed antiskyrmion size of 150 nm in Mn-Pt(Pd)-Sn based Heusler materials [28]. In the present case, by slightly changing the composition, both the magnetic anisotropy and the exchange interaction can be tuned significantly. This is evident from the increase in the coercive field and decrease in the T_C as

well as the saturation magnetic moment; which in principle could give rise to a reduced antiskyrmion size in $\text{Mn}_{2.1}\text{NiGa}_{0.9}$. Due to the ferrimagnetic ordering in the present system one can expect a reduced skyrmion Hall effect [47], that might help the present ferrimagnetic antiskyrmions to move along the direction of applied currents.

In summary, we have established the presence of a large topological Hall effect that withstands above room temperature in the Mn-Ni-Ga based magnetic shape memory alloys. The topological Hall effect that exists in the D_{2d} symmetry based tetragonal phase vanishes when the system undergoes a structural transition to the cubic phase. The origin of the observed THE is attributed to the presence of magnetic antiskyrmions. Owing to the large out-of-plane magnetic anisotropy in the present tetragonal phase, a detailed micromagnetic simulation was carried out to understand the stability of antiskyrmion phase in presence of different exchange interaction strength, anisotropy, and DMI. The present ferrimagnetic antiskyrmions with very high ordering temperatures possess a great potential for their application in *racetrack* memory devices as they are expected to display reduced skyrmion Hall effect in comparison to the ferromagnetic ones.

This work was financially supported by Department of Atomic Energy (DAE) and Department of Science and Technology (DST)-Ramanujan research grant (No. SB/S2/RJN-081/2016) of the Government of India.

* Authors contributed equally

† ajaya@niser.ac.in

- [1] S. S. P. Parkin, M. Hayashi, and L. Thomas, *Science* **320**, 190 (2008).
- [2] S. Mühlbauer, B. Binz, F. Jonietz, C. Pfleiderer, A. Rosch, A. Neubauer, R. Georgii, and P. Böni, *Science* **323**, 915 (2009).
- [3] X. Z. Yu, Y. Onose, N. Kanazawa, J. H. Park, J. H. Han, Y. Matsui, N. Nagaosa, and Y. Tokura, *Nature* **465**, 901 (2010).
- [4] T. Schulz, R. Ritz, A. Bauer, M. Halder, M. Wagner, C. Franz, C. Pfleiderer, K. Everschor, M. Garst, and A. Rosch, *Nature Phys.* **8**, 301 (2012).
- [5] N. Nagaosa and Y. Tokura, *Nature Nanotech.* **8**, 899 (2013).
- [6] J. C. Gallagher, K. Y. Meng, J. T. Brangham, H. L. Wang, B. D. Esser, D. W. McComb, and F. Y. Yang, *Phys. Rev. Lett.* **118**, 027201 (2017).
- [7] J. Matsuno, N. Ogawa, K. Yasuda, F. Kagawa, W. Koshihara, N. Nagaosa, Y. Tokura, and M. Kawasaki, *Sci. Adv.* **2**, e1600304 (2016).
- [8] N. Kanazawa, M. Kubota, A. Tsukazaki, Y. Kozuka, K. S. Takahashi, and M. Kawasaki, *Phys. Rev. B* **91**, 041122(R) (2015).
- [9] Yufan Li, N. Kanazawa, X. Z. Yu, A. Tsukazaki, M. Kawasaki, M. Ichikawa, X. F. Jin, F. Kagawa, and Y. Tokura, *Phys. Rev. Lett.* **110**, 117202 (2013).
- [10] S. X. Huang and C. L. Chien, *Phys. Rev. Lett.* **108**, 267201 (2012).
- [11] N. Kanazawa, Y. Onose, T. Arima, D. Okuyama, K. Ohoyama, S. Wakimoto, K. Kakurai, S. Ishiwata, and Y. Tokura, *Phys. Rev. Lett.* **106**, 156603 (2011).
- [12] A. Neubauer, C. Pfleiderer, B. Binz, A. Rosch, R. Ritz, P.G. Niklowitz, and P. Böni, *Phys. Rev. Lett.* **102**, 186602 (2009).
- [13] I. E. Dzyaloshinskii, *Sov. Phys. JETP* **5**, 1259 (1957).
- [14] T. Moriya, *Phys. Rev.* **120**, 91 (1960).
- [15] X. Z. Yu, N. Kanazawa, Y. Onose, K. Kimoto, W. Z. Zhang, S. Ishiwata, Y. Matsui, and Y. Tokura, *Nature Mater.* **10**, 106 (2011).
- [16] S. Seki, X. Z. Yu, S. Ishiwata, and Y. Tokura, *Science* **336**, 198 (2012).
- [17] Y. Tokunaga, X. Z. Yu, J. S. White, H. M. Ronnow, D. Morikawa, Y. Taguchi, and Y. Tokura, *Nature Comm.* **6**, 7638 (2015).
- [18] S. Heinze, K. von Bergmann, M. Menzel, J. Brede, A. Kubetzka, R. Wiesendanger, G. Bihlmayer, and Stefan Blügel, *Nature Phys.* **7**, 713 (2011).
- [19] J. Sampaio, V. Cros, S. Rohart, A. Thiaville, and A. Fert, *Nature Nanotech.* **8**, 839 (2013).
- [20] W. Jiang, P. Upadhyaya, W. Zhang, G. Yu, M. B. Jungfleisch, F. Y. Fradin, J. E. Pearson, Y. Tserkovnyak, K. L. Wang, O. Heinonen, S. G. E. te Velthuis, and A. Hoffmann, *Science* **349**, 283 (2015).
- [21] S. Woo, K. Litzius, B. Krüger, M.-Y. Im, L. Caretta, K. Richter, M. Mann, A. Krone, R. M. Reeve, M. Weigand, P. Agrawal, I. Lemesch, M.-A. Mawass, P. Fischer, M. Kläui, and G. S. D. Beach, *Nature Mater.* **15**, 501 (2016).
- [22] A. Soumyanarayanan, M. Raju, A. L. G. Oyarce, A. K. C. Tan, M.-Y. Im, A. P. Petrovic, P. Ho, K. H. Khoo, M. Tran, C. K. Gan, F. Ernult, and C. Panagopoulos, *Nature Mater.* **16**, 898 (2017).
- [23] I. Kezsmarki, S. Bordacs, P. Milde, E. Neuber, L. M. Eng, J. S. White, H. M. Ronnow, C. D. Dewhurst, M. Mochizuki, K. Yanai, H. Nakamura, D. Ehlers, V. Tsurkan and A. Loidl, *Nature Mater.* **14**, 1116 (2015).
- [24] T. Kurumaji, T. Nakajima, V. Ukleev, A. Feoktystov, T-hisa Arima, K. Kakurai, and Y. Tokura, *Phys. Rev. Lett.* **119**, 237201 (2017).
- [25] J. Li, A. Tan, K.W. Moon, A. Doran, M.A. Marcus, A.T. Young, E. Arenholz, S. Ma, R.F. Yang, C. Hwang, and Z.Q. Qiu, *Nature Comm.* **5**, 4704 (2014).
- [26] L. Sun, R. X. Cao, B. F. Miao, Z. Feng, B. You, D. Wu, W. Zhang, An Hu, and H. F. Ding, *Phys. Rev. Lett.* **110**, 167201 (2013).
- [27] B. F. Miao, L. Sun, Y. W. Wu, X. D. Tao, X. Xiong, Y. Wen, R. X. Cao, P. Wang, D. Wu, Q. F. Zhan, B. You, J. Du, R. W. Li, and H. F. Ding, *Phys. Rev. B* **90**, 174411 (2014).
- [28] A. K. Nayak, V. Kumar, T. Ma, P. Werner, E. Pippel, R. Sahoo, F. Damay, U. K. Rössler, C. Felser, and S. S. P. Parkin, *Nature* **548**, 561 (2017).
- [29] A. O. Leonov, and I. Kezsmarki, *Phys. Rev. B* **96**, 214413 (2017).
- [30] M. Hoffmann, B. Zimmermann, G. P. Mueller, D. Schuerhoff, N. S. Kiselev, C. Melcher, and S. Blügel, *Nature Comm.* **8**, 308 (2017).
- [31] L. Camosi, N. Rougemaille, O. Fruchart, J. Vogel, and S. Rohart, *Phys. Rev. B* **97**, 134404 (2018).
- [32] T. Graf, C. Felser, and S. S. P. Parkin, *Prog. Solid State*

- Chem.* **39**, 1 (2011).
- [33] O. Meshcheriakova, S. Chadov, A. K. Nayak, U. Roessler, J. Kuebler, J. Kiss, G. Andre, A. A. Tsirlin, S. Hausdorf, A. Kalache, W. Schnelle, M. Nicklas, and C. Felser, *Phys. Rev. Lett.* **113**, 087203 (2014).
 - [34] A. K. Nayak, C. Salazar Mejia, S. W. D'Souza, S. Chadov, Y. Skourski, C. Felser, and M. Nicklas, *Phys. Rev. B* **90**, 220408(R) (2014).
 - [35] A. Planes, L. Maanosa, and Mehmet Acet, *J. Phys.: Cond. Mat.* **21**, 233201 (2009).
 - [36] G-H. Yu, Y-L. Xu, Z-H. Liu, H-M. Qiu, Z-Y. Zhu, X-P. Huang, L-Q. Pan, *Rare Met.* **34**, 527 (2015).
 - [37] G. D. Liu, J. L. Chen, Z. H. Liu, X. F. Dai, G. H. Wua, B. Zhang, and X. X. Zhang, *Appl. Phys. Lett.* **87**, 262504 (2005).
 - [38] G. D. Liu, X. F. Dai, S. Y. Yu, Z. Y. Zhu, J. L. Chen, G. H. Wu, H. Zhu, and J. Q. Xiao, *Phys. Rev. B* **74**, 054435 (2006).
 - [39] B. Balke, G. H. Fecher, J. Winterlik, and C. Felser, *Appl. Phys. Lett.* **90**, 152504 (2007).
 - [40] A. K. Nayak, M. Nicklas, S. Chadov, P. Khuntia, C. Shekhar, A. Kalache, M. Baenitz, Y. Skourski, V. K. Guduru, A. Puri, U. Zeitler, J. M. D. Coey, and C. Felser, *Nature Mater.* **14**, 679 (2015).
 - [41] S. R. Barman and A. Chakrabarti, *Phys. Rev. B* **77**, 176401 (2008).
 - [42] M.J. Donahue, D.G Porter OOMMF User's Guide, Version 1.0, Interagency Report NISTIR, 2009.
 - [43] S. Rohart, A. Thiaville DMExchange6Ngbr, <http://math.nist.gov/oommf/contrib/oxsext>, 2012.
 - [44] H. Wilhelm, M. Baenitz, M. Schmidt, U. K. Rössler, A. A. Leonov, and A. N. Bogdanov, *Phys. Rev. Lett.* **107**, 127203 (2011).
 - [45] A. Bauer and C. Pfleiderer, *Phys. Rev. B* **85**, 214418 (2012).
 - [46] Sk. Jamaluddin, S. K. Manna, B. Giri, P. V. Prakash Madduri, S.S. P. Parkin, and A. K. Nayak, *Adv. Funct. Mater.* (2019), DOI: 10.1002/adfm.201901776
 - [47] S. Woo, K. M. Song, X. Zhang, Y. Zhou, M. Ezawa, X. Liu, S. Finizio, J. Raabe, N. J. Lee, S. Kim, S.-Y. Park, Y. Kim, J.-Y. Kim, D. Lee, O. Lee, J. W. Choi, B.-C. Min, H. C. Koo, and J. Chang, *Nature Comm.* **9**, 959 (2018).